Electronic Supplementary Material (ESI) for Journal of Materials Chemistry A.

Facile Room Temperature Solventless Synthesis of High Thermoelectric Performance Ag_2Se via Dissociative Adsorption Reaction

Dongwang Yang[a], Xianli Su[a,e*], Fanchen Meng[b], Si Wang[a,d], Yonggao Yan[a], Jihui Yang[c], Jian He[b], Qingjie Zhang[a], Ctirad Uher[d], Mercouri G. Kanatzidis[e*] and Xinfeng Tang[a*]

[a]*State Key Laboratory of Advanced Technology for Materials Synthesis and Processing, Wuhan University of Technology, Wuhan 430070, China.*
[b]*Department of Physics and Astronomy, Clemson University, Clemson, South Carolina 29634, USA.*
[c]*Materials Science and Engineering Department, University of Washington, Seattle, Washington98195, USA.*
[d]*Department of Physics, University of Michigan, Ann Arbor, Michigan48109, USA.*
[e]*Department of Chemistry, Northwestern University, Evanston, Illinois 60208, USA*

Correspondence and requests for materials should be addressed to Xianli Su (suxianli@whut.edu.cn), Mercouri G. Kanatzidis (m-kanatzidis@northwestern.edu) or to Xinfeng Tang (tangxf@whut.edu.cn)

1. Experiments

Exploration of the reaction mechanism: **Figures S1**(a) and S1(b) depict the microstructure of raw Ag and Se powders before the reaction. The particle size is on the scale of micrometers. Cracks tend to develop on the surface of Ag particles shortly after Ag physically contacts with Se (Figure S1(c)). In the meantime, fine particles with sizes from a few to hundreds of nanometers form, as shown in Figure S1(d). EDS results confirmed that the as-formed fine particles are the Ag_2Se compound. Upon grinding, these Ag_2Se nanoparticles easily fell off the surface of Ag grains and the newly exposed fresh surface of Ag continued to react with Se to form Ag_2Se (Figure S1(e)) until all reactants were spent.

To help understand the underlying reaction mechanism, we have designed and conducted a series of experiments. The first experiment consisted of three parts. In the first part, we embedded a 1 mm diameter Ag rod in a pile of Se powder for 16 h at ambient conditions. The resulting surface morphology exhibited pits and clusters of Ag_2Se nanoparticles (**Figure S2**), a situation resembling corrosion or etching. In the second part, we loosely piled Ag powder on the surface of a dense piece of Se. After 1 h at ambient conditions, we brushed off the Ag powder and found that there were some Ag micron-size particles remaining on the Se surface with a clear interface between Ag and Se (**Figure S3**). Interestingly, the upper surface of Ag particles was covered with nanoparticles. Other than these, the exposed Se surface was very clean. In the third part, we loosely piled Se powder on the surface of a plate of Ag made of cold-pressed Ag powder. We intentionally let the powder of Se covering only one half of the surface area and left the other half uncovered (**Figure S4** and **S5**). After the exposure of 1 h at ambient conditions, we removed the Se powder carefully by a vacuum cleaner and inspected the surface micro-morphology of the Ag plate by means of SEM and EDS. We found that a multitude of Ag_2Se nanoparticles have formed on the covered surface area, and they agglomerated into networks. The surface micro-morphology of the Se-covered Ag plate looked like a corroded surface. Surprisingly, we also found a substantial number of Ag_2Se nanoparticles on the Ag surface not covered with the Se powder, and they became less numerous with increasing distance from the borderline between the covered and uncovered areas. The latter observation strongly suggests the presence of Se vapor in the reaction process.

To shed light on this phenomenon, we conducted a second experiment consisting of 3 parts. In the first part, a plate of Ag was placed 1 cm above a pile of Se powder at ambient conditions for 12.5 h (**Figure S6**). We found the bottom surface of the Ag plate covered by Ag_2Se nanoparticles (the inset of Figure 1(d)), although at a much smaller yield than in the previous experiments. Apparently, the Ag plate reacted with the Se vapor. The resulting micro-morphology is reminiscent of a nanomaterial grown by chemical vapor deposition[1, 2] on an etched substrate. In the second and third parts of the experiment, a plate of Ag was placed above a pile of Se in vacuum for 11 h (**Figure**

S7) and, respectively, in Se vapor produced by heating the Se powder for 5 s (**Figure S8**). Both Ag plates showed similar micro-morphology as one might expect from the chemical vapor deposition process. However, due to the more intense reaction in Se vapor, XRD results indicated a more pronounced presence of Ag_2Se.

Interestingly, when we partly embedded the Ag plate into the Te or S powder for 1 h, there exists similar phenomenon between Ag and Se, Te or S. As shown in **Figure S9**, the surface micro-morphology of the Te / S-embedded Ag plate looked like a corroded surface, and some nanoparticles experienced on the exposed area. While the degree of corrosion of Ag with Te is much more serious than Ag with S.

Detection of the reaction heat: the heat content of the reaction was measured using a microcalorimeter (C80, Setaram, France) operated under the constant temperature mode and the membrane mixing pool, with Ag powder (200 mesh) placed on the membrane and Te powder, Se powder or S powder (200 mesh) located under the membrane. The total mass of the stoichiometric admixture was 1 g. To minimize the thermal effect caused by stirring, Al_2O_3 powder (200 mesh) of equal mass was put into another mixing pool as a reference. After maintaining the constant temperature for two hours, the membrane was pierced by the stirring rod, at which point a built-in high-sensitivity 3D sensor started to measure the reaction heat during stirring. As shown in Figure 1(b) and **Figure S10**, an exothermic signal was observed after mixing Ag with Te/Se/S, along with a slight increase in the ambient temperature. Combined with the morphology analysis, we can conclude that the reaction rate is $Ag_2Te > Ag_2Se > Ag_2S$.

Synthesis of the cold pressed samples： 26 g of Ag (3N, 200 mesh, Sinopharm Chemical Reagent Co., China) and Se (5N, 200 mesh, Mount Emei semiconductor factory, China) powders were weighed according to the stoichiometric ratio. Single phase Ag_2Se was obtained by gently grinding for 30 min. Subsequently, the reacted powder was cold pressed into pellets at a pressure of 450MPa for 2 min. The resulting pellet with the diameter of 20 mm and the height of 10 mm had a relative density of more than 99% and was practically isotropic. The ingot was cut into different shapes for the thermoelectric property measurements.

Synthesis of the melt-grown+SPS processed samples： stoichiometric amounts of high purity filamentary silver (5N, Sinopharm Chemical Reagent Co., China) and selenium chunks (5N, Mount Emei semiconductor factory, China) were weighed and sealed in a silica tube under a pressure of 10^{-3} Pa. Subsequently, the tube was slowly heated up to 1273 K and maintained there for 12 h, followed by furnace cooling to room temperature. Finally, the obtained ingot was ground into a fine powder and consolidated using spark plasma sintering (SPS) (SPS1050, Sumimoto, Japan) at 713 K for 2 min under a pressure of 30 MPa. The relative density of the resulting pellets, having the diameter of 10 mm and the height of 10 mm, was higher than 98%.

Phase, morphology and thermoelectric properties： The electrical conductivity

and the Seebeck coefficient were measured on bar-shaped samples cut along both the perpendicular and the parallel directions with respect to the pressing direction. Transport measurements were conducted using an ULVAC-RIKO ZEM-3 (Ulvac, Japan) instrument under a helium atmosphere from 300 K to 390 K. The electrical conductivity (σ) and the Hall coefficient (R_H) between 10 K and 300 K were measured on a Physical Properties Measurement System (PPMS-9, Quantum Design, USA). The effective carrier concentration (n_H) was calculated by the formula: $n_H=1/eR_H$, where e is the electron charge. The Hall mobility follows from $\mu_H=\sigma R_H$. The thermal conductivity was calculated using the relation $\kappa=D\times C_p\times\rho$, where the thermal diffusivity D was measured using a LFA457 (Netzsch, Germany) laser flash apparatus. Thermal diffusivity (D) measurements were performed on square-shaped samples cut along the corresponding directions to ensure that *all TE properties were measured in the same direction*. High temperature specific heat capacity C_p was measured using Q2000 (TA, USA). The uncertainties were estimated to be 3% for thermal diffusivity, specific heat capacity, and electrical conductivity, and 5% for the Seebeck coefficient, which results in an uncertainty of 4%, 10%, 11% for the thermal conductivity, power factor, and ZT, respectively. To increase the readability of all the curves, all figures are plotted without error bars.

Phase purity of all samples was inspected by X-ray powder diffraction (Empyrean, Cu K_α line, PANalytical, Holland). Images of freshly fractured surfaces were taken by field emission scanning electron microscopy (FESEM) (SU8000, Hitachi, Japan) with energy-dispersive X-ray spectroscopy (EDS) (XFlash6160, BRUKER, Germany). Back-scattered images were taken by EPMA (JXA-8100, JEOL, Japan).

2. Theory calculations

Chemical hardness calculations: We calculated the chemical hardness of Ag, O, S, Se, Te. The calculations were performed using the widely used Gaussian ® 09 software.[3] The post-HF method, namely, MP2 along with the Def2-QZVPPD[4] basis sets were employed to calculate the energetics of the atoms (Ag, O, S, Se and Te). The chemical hardness η was calculated by the following formula:

$$\eta \approx \frac{I-A}{2} \tag{1}$$

where I is the ionization energy and A is the electron affinity. [5]

There are two ways to estimate the values of I and A. The first approach is based on the Koopmans' theorem, [6] which connects frontier orbital energies with I and A. The negative energy of the highest occupied molecular orbital (HOMO) is regarded as I, while the negative energy of the lowest unoccupied molecular orbital (LUMO) is regarded as A. The other approach is the so-called "direct" method, using the following definition:

$$I = E_{X^+} - E_X \tag{2}$$

$$A = E_{X^-} - E_X \quad (3)$$

where E_{X^+}, E_{X^-} and E_X are the energies of an atom that lost one electron, that gained one electron and a charge neutral atom, respectively.

As shown in **Table S1**, the calculated "chemical hardness" using the direct method is in good agreement with the experimental values. The results of both methods agree on the same trend.

It can be seen that the chemical hardness of chalcogen elements, from large to small, is O, S, Se, Te. They attract electrons in the reaction, thus belonging to the Lewis acids[9]. As Ag losses electrons in the reaction, it belongs to the Lewis bases [9]. The hardness of Ag is 3.21, relatively soft. According to the theory of *Hard Soft Acid Base* (HSAB), a soft acid tends to form stable compounds with a soft base in thermodynamics and kinetics[9, 10]. Thus, Ag tends to react with Te to generate a stable compound Ag_2Te, followed by Ag reacting with Se and S to form Ag_2Se and Ag_2S, respectively. The reaction rate also follows the same trend. On the other hand, O is a hard Lewis acid, the compound Ag_2O, formed with Ag is not stable, which is consistent with previous research results[11].

Table S1 Calculated I and A values with the "direct" method and the experimental values. Calculated η values with both methods and the experimental values.

	I	I_{exp}[7]	A	A_{exp}[8]	η_1	η_2	η_{exp}[5]
Ag	7.46	7.58	1.05	1.30	3.65	3.21	3.14
O	13.41	13.62	1.44	1.46	9.72	5.98	6.08
S	10.08	10.36	1.98	2.08	6.51	4.05	4.14
Se	9.43	9.75	1.97	2.02	6.08	3.73	3.87
Te	8.5	9.01	1.95	1.97	5.29	3.27	3.52

η_1 is obtained with the energies of frontier orbitals.

η_2 is obtained with the calculated value of I and A.

Density functional theory calculations: The density functional theory (DFT) calculations were carried out using the Cambridge Sequential Total Energy Package (CASTEP) code[12] of Materials Studio 8.0. We used the exchange-correlation functional based on the generalized gradient approximation (GGA) in the PBESol scheme. Ultra-soft pseudopotentials and a plane wave basis set were employed in this work. The plane-wave cutoff energy was 450 eV. All structures were relaxed until the forces acting on each atom were less than 0.01 eV/Å.

First, the structure of a silver crystal was calculated using the methods mentioned above with a (11× 11× 11) k-point mesh. The calculated lattice parameters for silver are a = b = c = 4.061 Å and $\alpha = \beta = \gamma = 90°$, in good accord with our experimental values a = b = c = 4.087 and $\alpha = \beta = \gamma = 90°$. In addition, the structure of a Se dimer[13] (Se_2) was

also calculated. In the calculation of Se_2, only gamma point was used in the k-point sampling. The calculated bond length was 2.153 Å, agreeing very well with the experimental value of 2.166 Å.[14]

In order to investigate the surface properties of the silver crystal, major facets (001), (011) and (111) were cleaved from the optimized silver crystal[15, 16] and the vacuum layer was at least 10 Å to avoid any image interaction. A super cell of $3 \times 3 \times 1$ was built for the silver surfaces. $(5 \times 5 \times 1)$ k-point mesh for the (001) and (111) surfaces and $(3 \times 5 \times 1)$ k-point mesh for the (011) surface were employed in the calculation. All modeled surfaces consist of five silver layers. The inner two layers were kept fixed and the outer three layers were allowed to relax. In order to find the optimal adsorption sites for Se_2 on Ag(001), Ag(011) and Ag(111) surfaces, a large number of initial adsorption sites were tested, and then the structure was left to relax until convergence criteria was met.

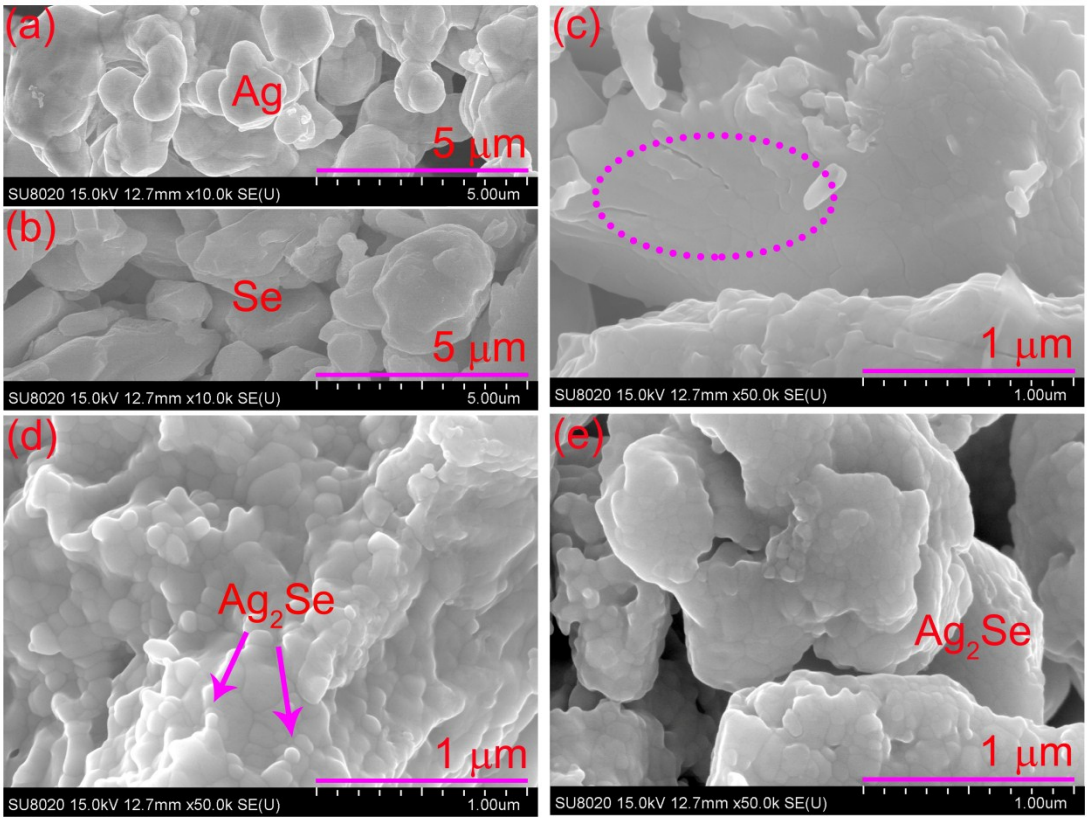

Figure S1. FESEM: (a) Ag powder, (b) Se powder, (c) "2Ag+Se" powder before grinding, (d) "2Ag+Se" powder during grinding, (e) phase pure Ag_2Se product. Cracks tend to develop on the surface of Ag particles shortly after Ag physically contacts with Se (Figure (c)). In the meantime, fine particles with sizes from a few to hundreds of nanometers form, as shown in Figure (d). EDS results shows that the as-formed fine particles are the Ag_2Se compound. Upon grinding, these Ag_2Se nanoparticles easily fall off the surface of Ag grains and the newly exposed fresh surface of Ag continues to react with Se to form Ag_2Se (Figure (e)) until all reactants are exhausted.

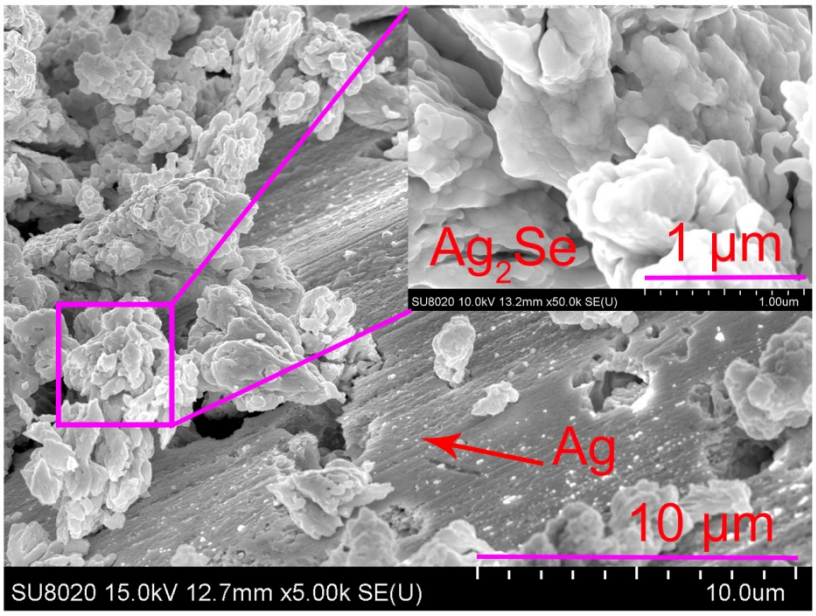

Figure S2. FESEM image of the micromorphology of a rod of Ag embedded in a pile of Se powder for 16 h. The surface morphology exhibited pits and clusters of Ag_2Se nanoparticles, a situation resembling corrosion or etching.

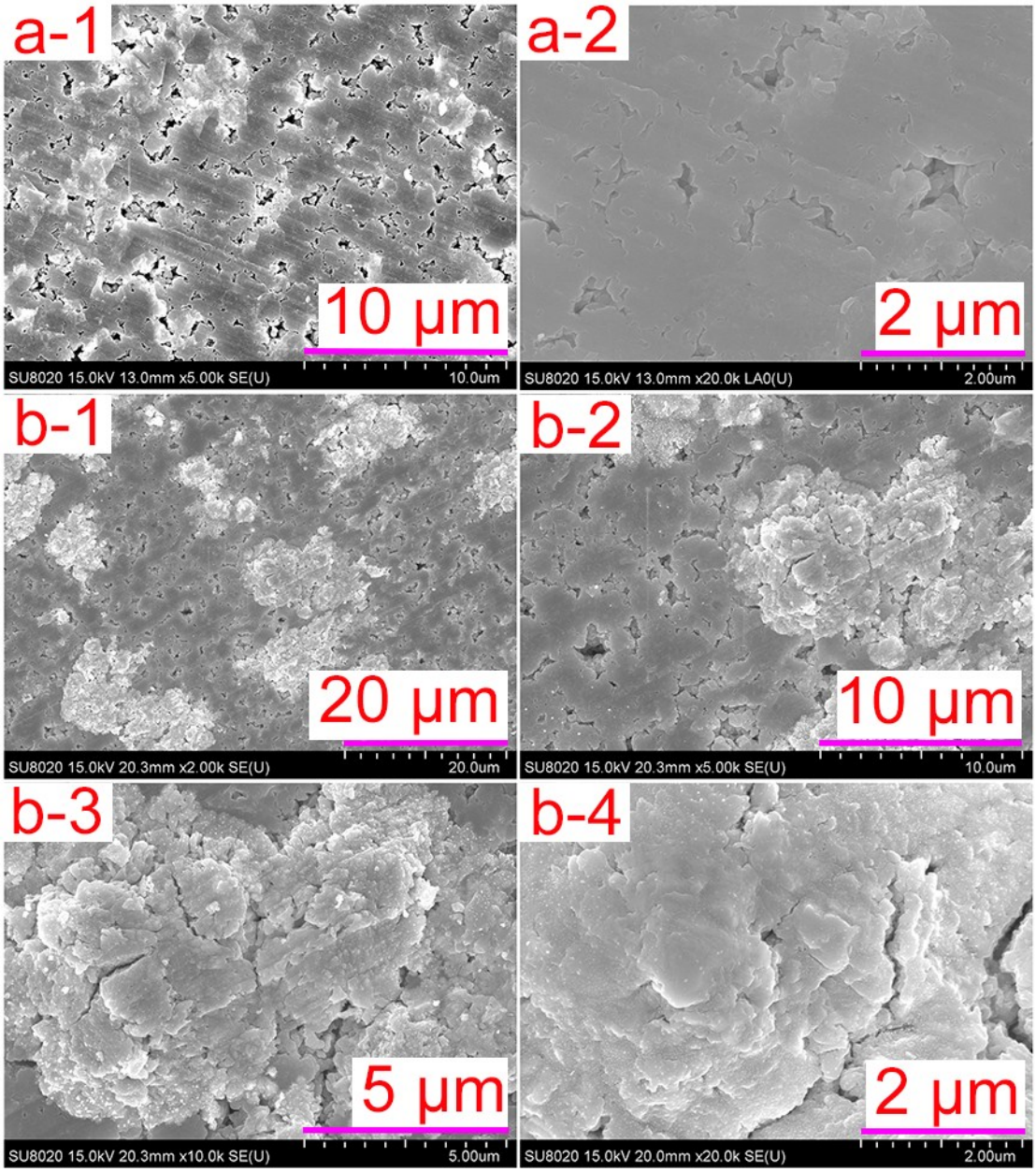

Figure S3. FESEM images of the surface micromorphology of a dense piece of Se: (a) pure Se piece, the magnification of image a-1 and a-2 is 5 k and 20 k; (b) Se piece covered with Ag powder for 1 h, the magnification of image b-1, b-2, b-3 and b-4 is 2 k, 5 k, 10 k and 20 k, respectively. The surface of pure Se piece is very clean (Figure a). When the Ag powder was brushed off after 1 h, there were also some Ag micron-size particles remaining on the Se surface with a clear interface between Ag and Se (Figure b). Interestingly, the upper surface of Ag particles was covered with nanoparticles. Other than these, the exposed Se surface was very clean.

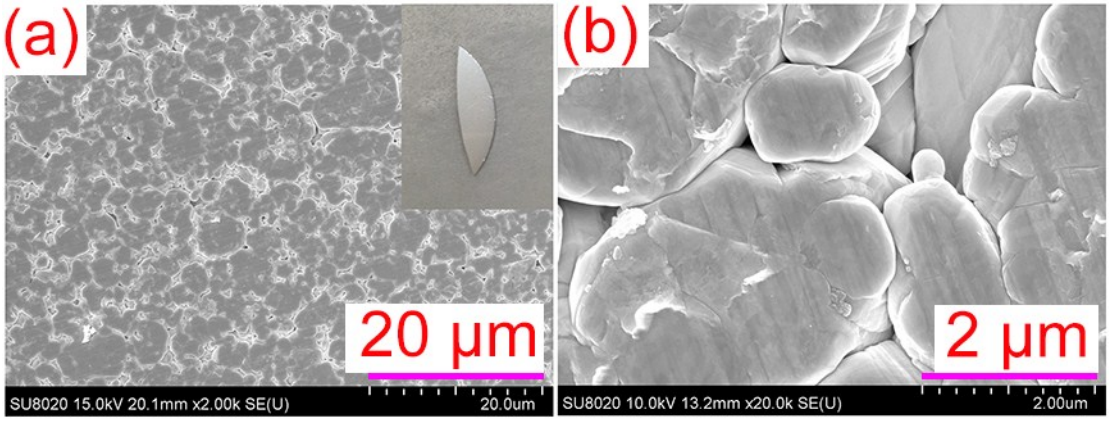

Figure S4. FESEM images of the surface micromorphology of the Ag plate compacted by cold-pressing Ag-powder. The magnification of image (a) and (b) is 2 k and 20 k. The surface of pure Ag plate is very clean.

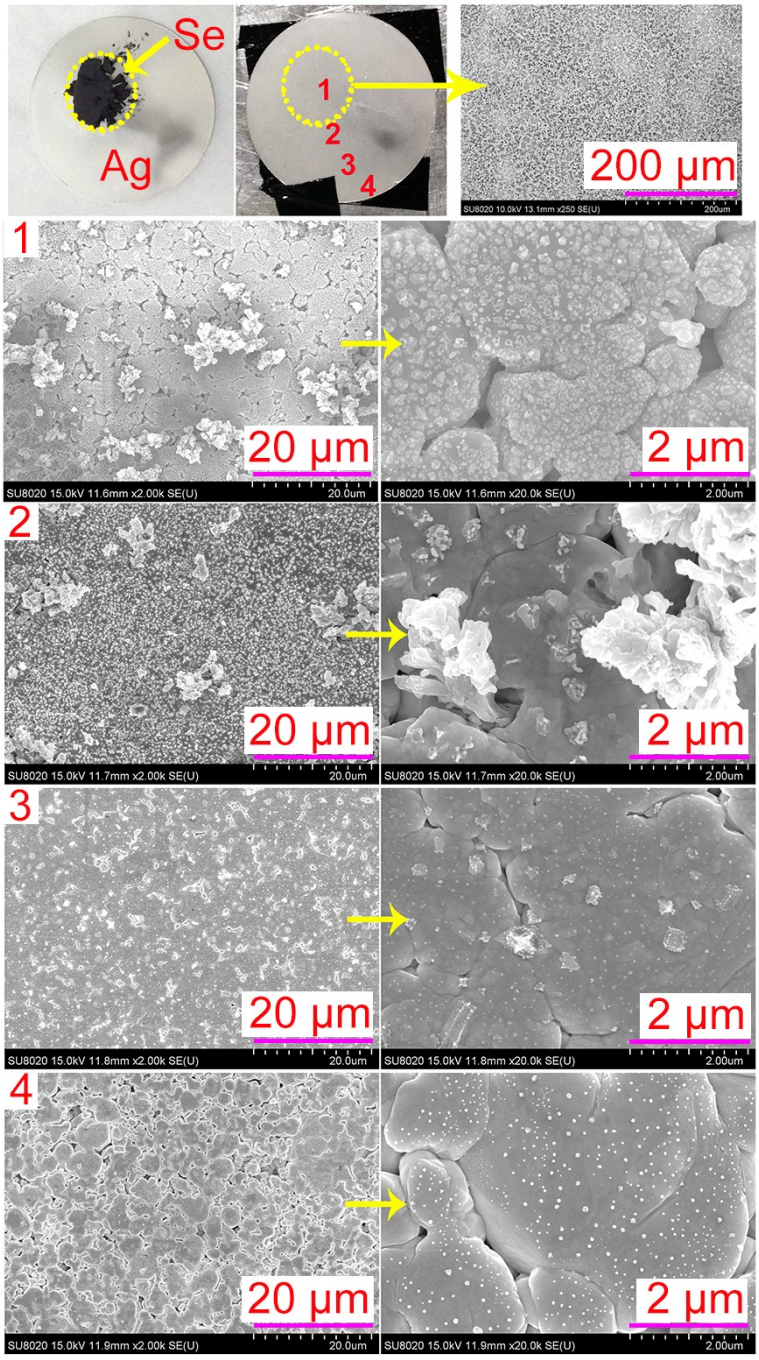

Figure S5. FESEM images of the surface micromorphology at various points labeled 1, 2, 3, and 4 of the Ag plate partly covered with Se powder for 1 h. The arrow indicates image magnification. A multitude of Ag_2Se nanoparticles have formed on the covered surface area, and they agglomerated into networks. The surface micro-morphology of the Se-covered Ag plate looked like a corroded surface. Surprisingly, a substantial number of Ag_2Se nanoparticles also formed on the Ag surface not covered with the Se powder, and they became less numerous with increasing distance from the borderline between the covered and uncovered areas, i.e. from point 1 to point 4. The latter observation strongly suggests the presence of Se vapor in the reaction process.

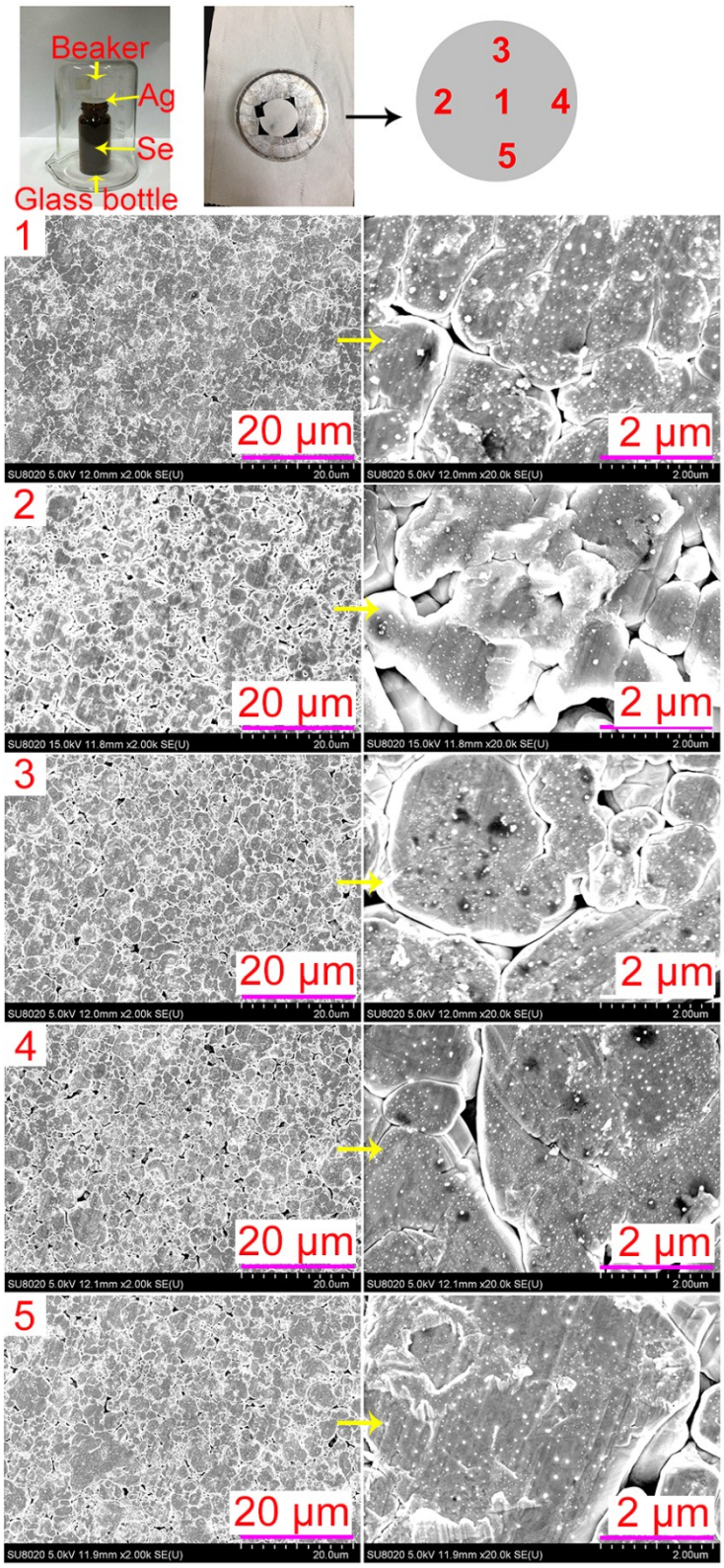

Figure S6. FESEM images of the micromorphology at various points labeled 1, 2, 3, 4, and 5 of the bottom surface of the Ag plate placed 1 cm above a pile of Se powder at ambient conditions for 12.5 h. The arrow indicates image magnification. The bottom surface of the Ag plate was covered by Ag_2Se nanoparticles. Apparently, the Ag plate reacted with the Se vapor.

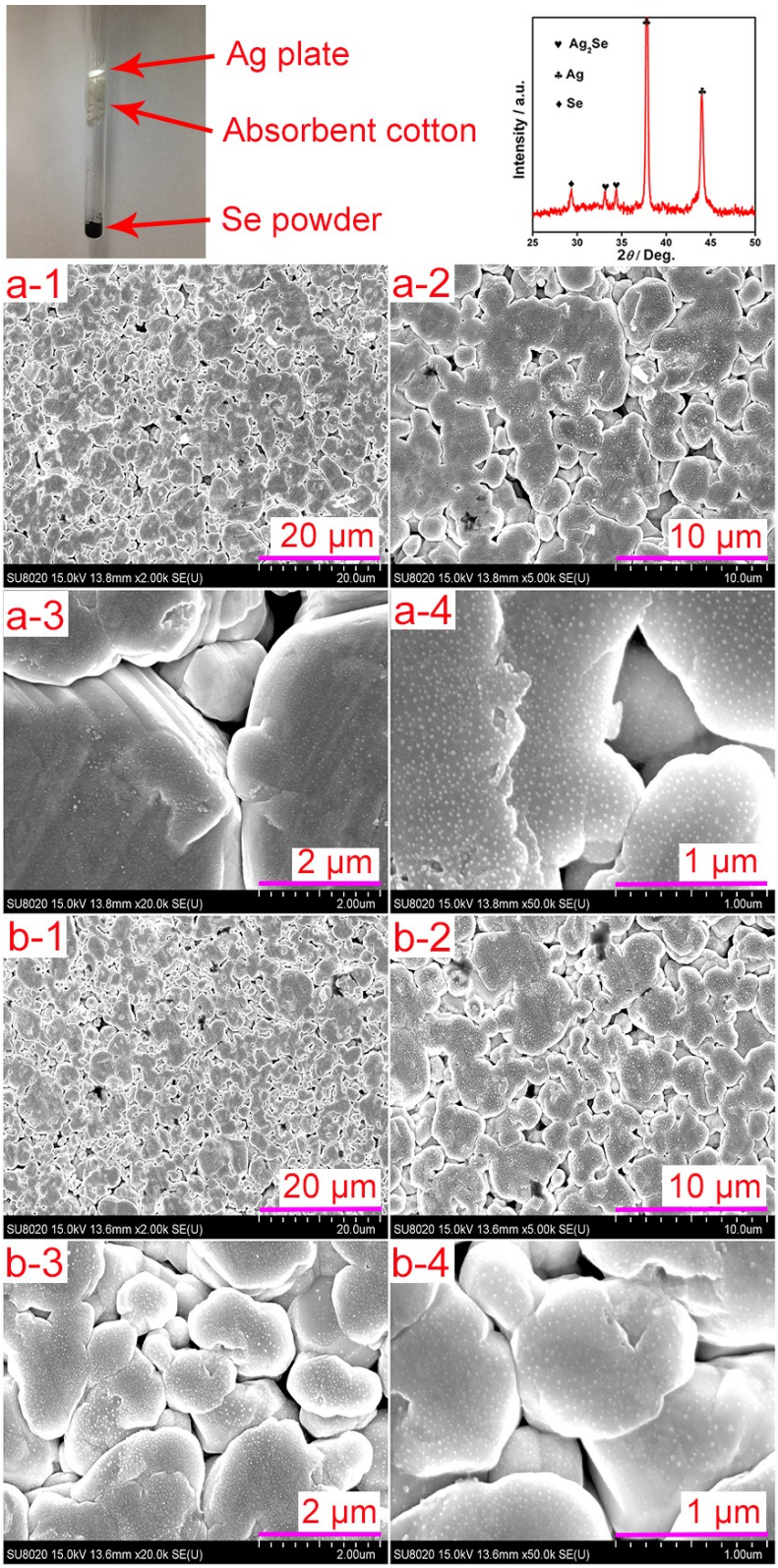

Figure S7. XRD pattern and FESEM images of the micromorphology of both surfaces of the Ag plate placed above a pile of Se powder in vacuum for 11 h: (a) one side, the magnification of image a-1, a-2, a-3 and a-4 is 2 k, 5 k, 20 k and 50 k, respectively; (b) the other side, the magnification of image b-1, b-2, b-3 and b-4 is 2 k, 5 k, 20 k and 50 k, respectively. Both surface of the Ag plate were covered by Ag_2Se nanoparticles.

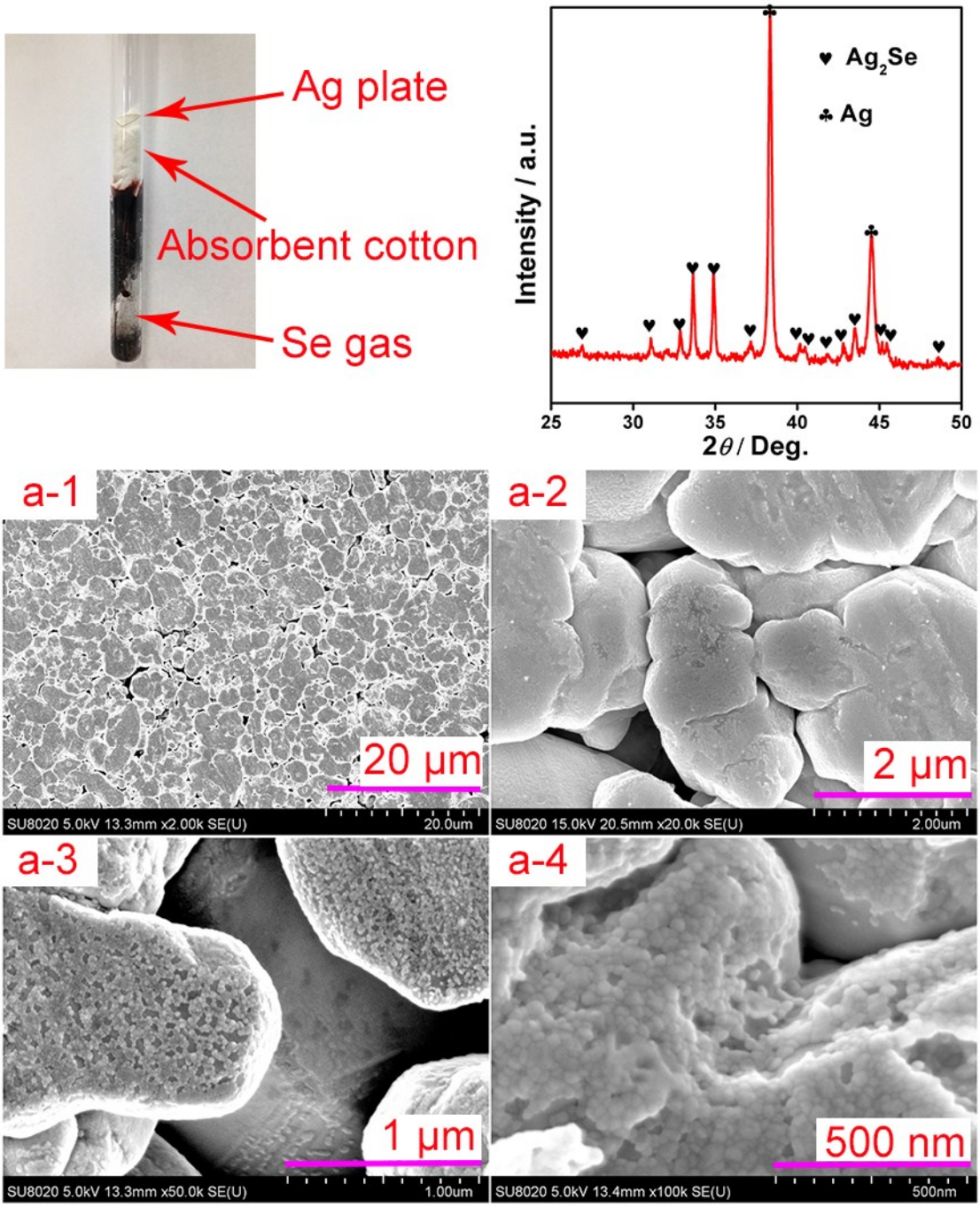

Figure S8. XRD pattern and FESEM images of the micromorphology of the Ag plate surface exposed to Se vapor for 5 s. the magnification of image a-1, a-2, a-3 and a-4 is 2 k, 20 k, 50 k and 100 k, respectively. Ag plates showed similar micro-morphology as one might expect from the chemical vapor deposition process.

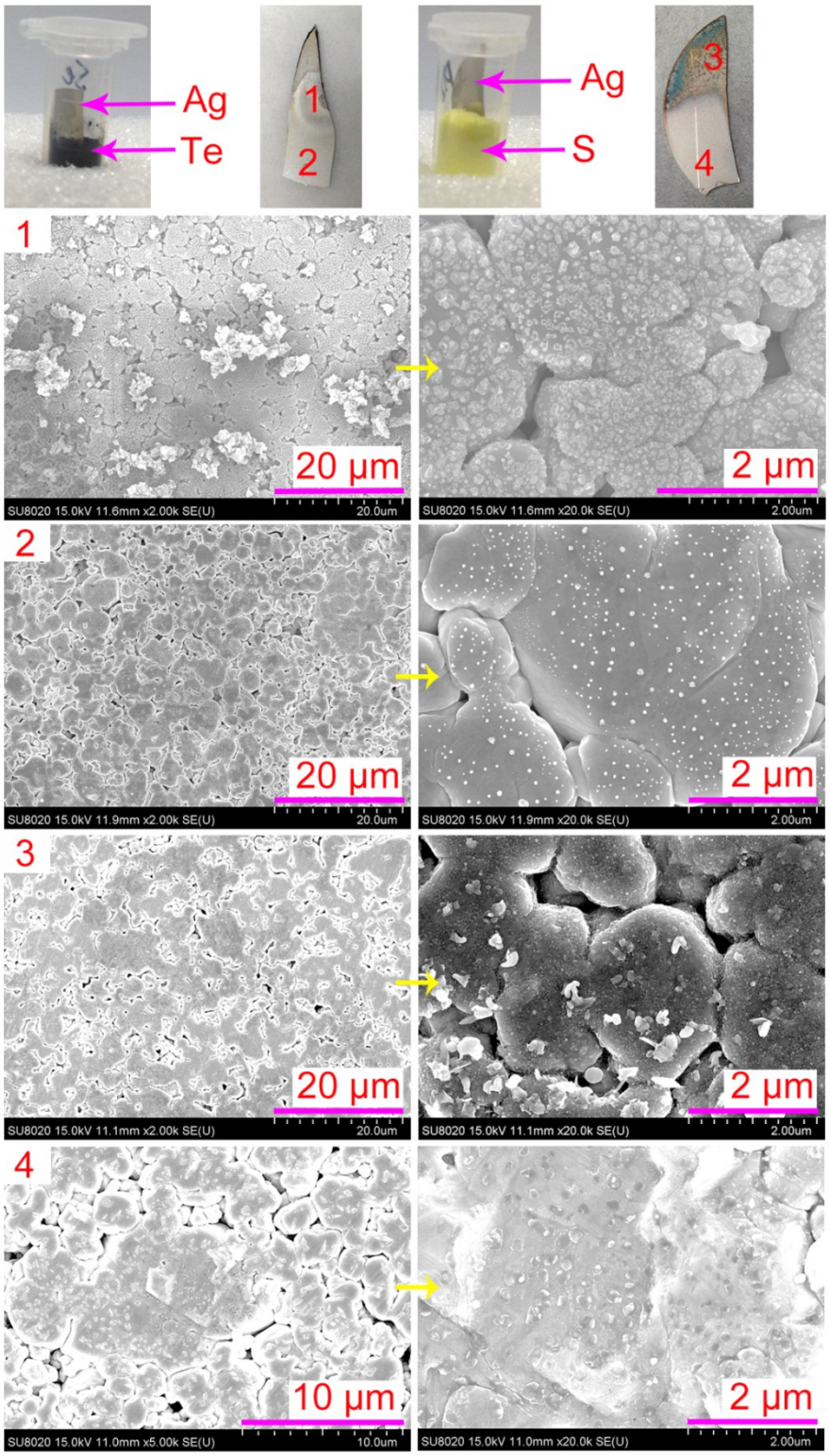

Figure S9. FESEM images of the surface micromorphology at various points of the Ag plate partly embedded into Te and S powder for 1 h. Position 1 and 3 are the parts of Ag plate embedded into the powder, while position 2 and 4 are the exposed parts of Ag plate. the surface micro-morphology of the Te / S-embedded Ag plate looked like a corroded surface, and some nanoparticles experienced on the exposed area. While the degree of corrosion of Ag with Te is much more serious than Ag with S.

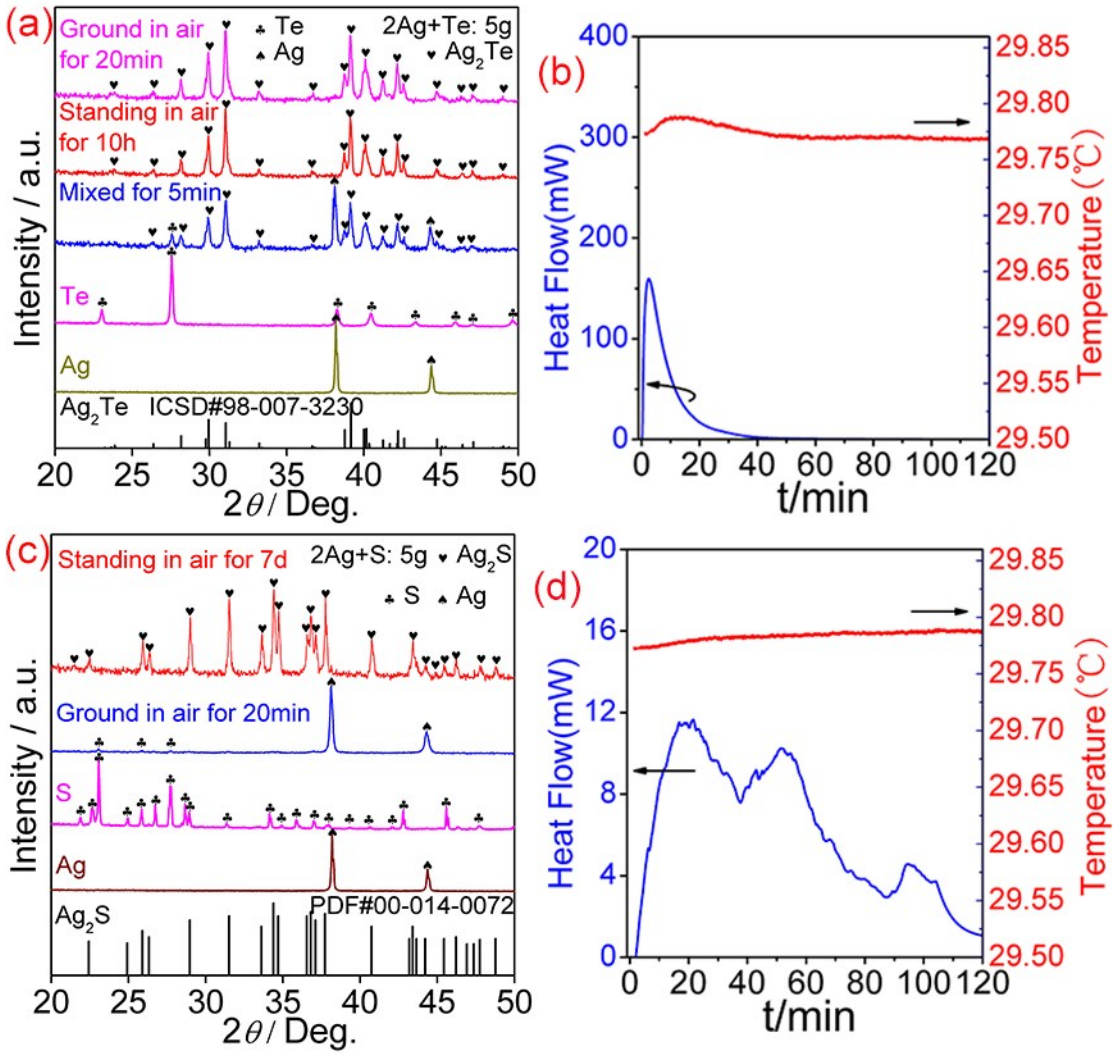

Figure S10. (a) XRD patterns after mixing / grinding a stoichiometric powder, 2Ag+Te, for various durations; (b) heat flow and temperature change curve during mixing of 2Ag+Te as a function of time; (c) XRD patterns after grinding a stoichiometric powder, 2Ag+S, for various times; (d) heat flow and temperature change curve during mixing of 2Ag+S as a function of time.

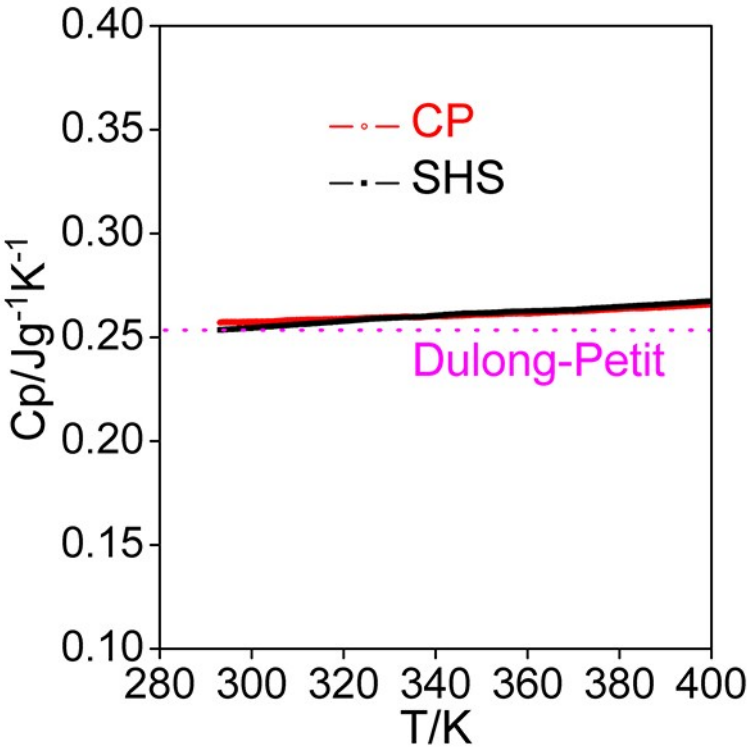

Figure S11. Heat capacity of Ag_2Se. The Dulong-Petit limit is shown in the dotted line.

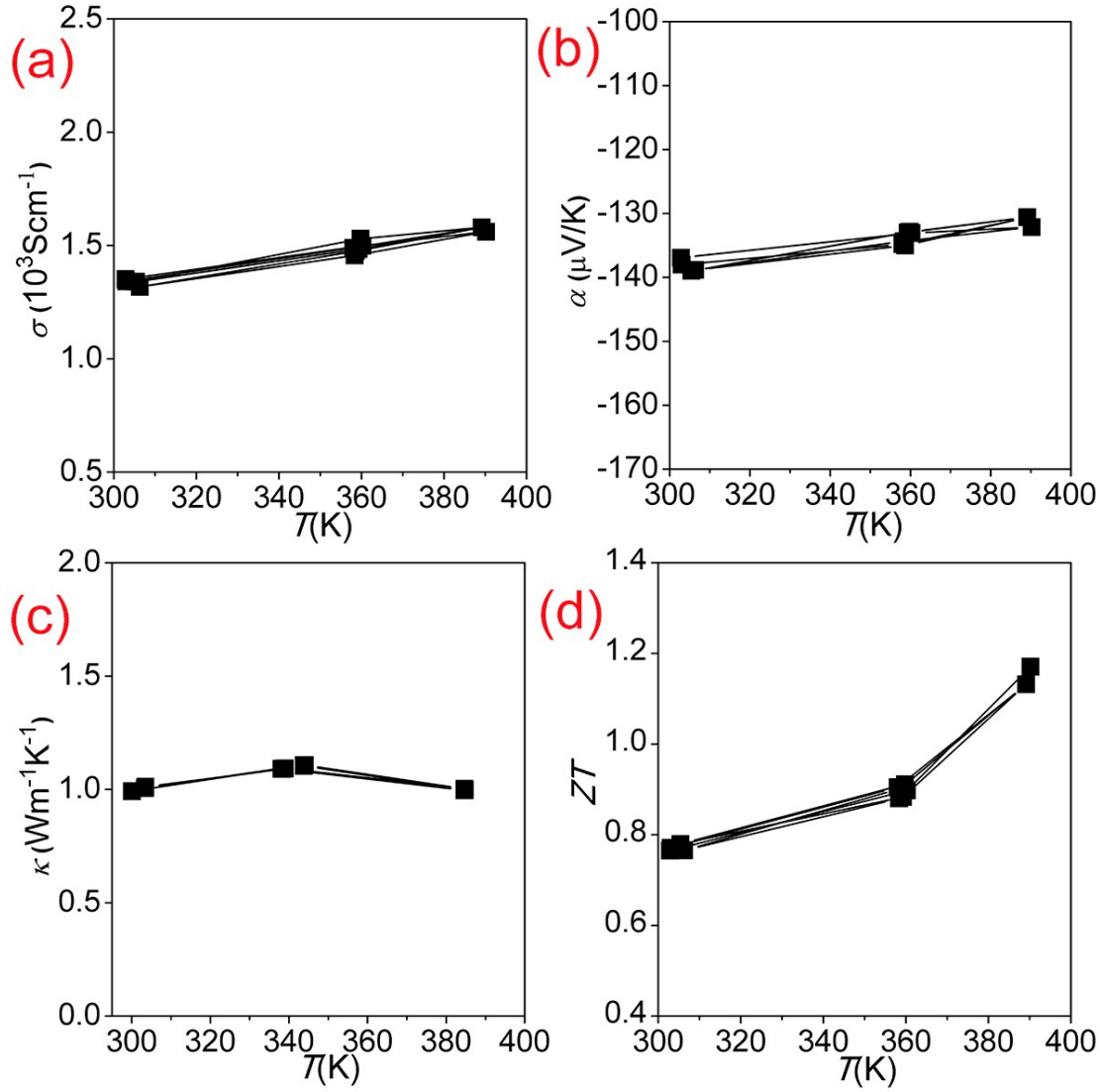

Figure S12. Thermoelectric properties of the CP sample after 6 thermal cycles between room temperature and 390 K.

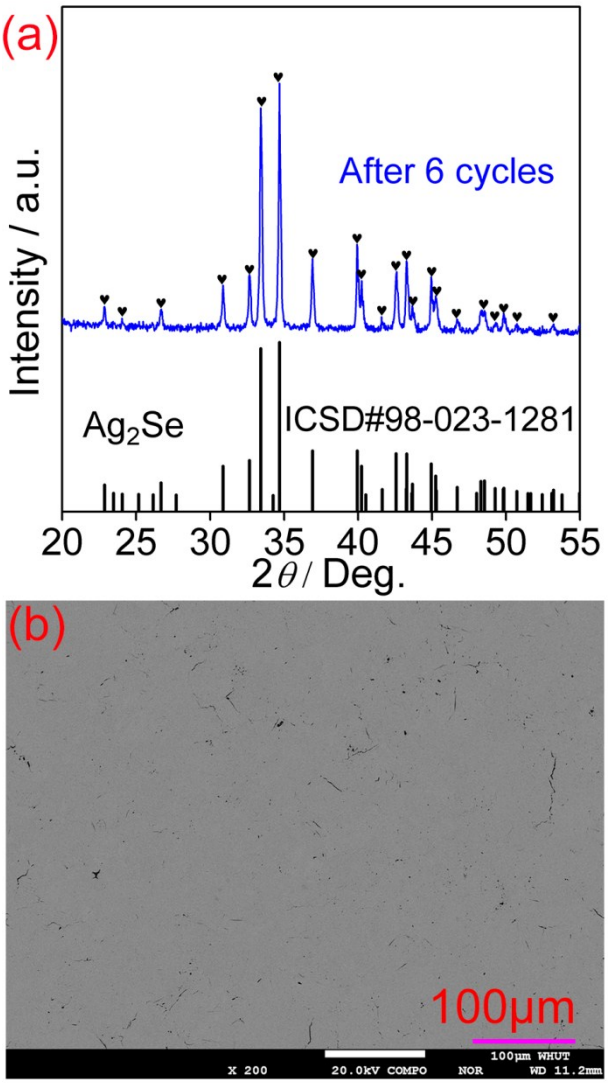

Figure S13. PXRD pattern and a back-scattering EPMA image of the CP sample after 6 thermal cycles between room temperature and 390 K.

References:

1 J. J. Wu and S. C. Liu, *Adv. Mater.* **2002**, 14, 215-218.

2 M. Chhowalla, K. B. K. Teo, C. Ducati, N. L. Rupesinghe, G. A. J. Amaratunga, A. C. Ferrari, D. Roy, J. Robertson and W. I. Milne, *J. Appl. Phys.* **2001**, 90, 5308-5317.

3 M. J. Frisch, G. W. Trucks, H. B. Schlegel, G. E. Scuseria, M. A. Robb and J. R. Cheeseman, GAUSSIAN 09. B.01 ed., Gaussian, Inc., Wallingford, CT, **2009**.

4 D. Rappoport and F. Furche, *J. Chem. Phys*. **2010**, 133, 366-369.

5 R. G. Pearson, *J. Org Chem*, **1988**, 27, 734-740.

6 T. Koopmans, *Physica*, **1934**, 1, 104-113.

7 C. E. Moore, *Account*. *Hist*. *Rev*., **2001**, 11, 349-368.

8 H. Hotop and W. C. Lineberger, *J. Phys. Chem. Ref. Data*, **1975**, 14, 731-750.

9 R. G. Pearson, *J. Am. Chem. Soc.***1963**, 85, 3533-3539.

10 P. K. Chattaraj and P. V. R. Schleyer, *J. Am. Chem. Soc.* **1994**, 116, 1067-1071.

11 W. Tiano, M. Dapiaggi and G. Artioli, *J. Appl. Cryst.* **2003**, 36, 1461-1463.

12 S. J. Clark, M. D. Segall, C. J. Pickard, P. J. Hasnip, M. J. Probert and K. Refson, *Z. Kristallogr.* **2005**, 220, 567-570.

13 J. J. Li, H. X. Wang, L. Wu, C. Chen, Z. Q. Zhou, F. F. Liu, Y. Sun, J. B. Han and Y. Zhang, *ACS Appl. Mater. Interfaces* **2016**, 8, 10283-10292.

14 G. Hcrzberg, *Molecular Spectra and Molecular Structure, Vol. IV*. *Constants of Diatomic Molecules*. In Van Noslrand-Reinhold, New York: **1979**.

15 A. W. Czanderna, *Acta* **1978**, 24, 359-367.

16 C. Backx, J. Moolhuysen, P. Geenen and R. A. V. Santen, *J. Catal.* **1981**, 72, 364-368.